A scattering and absorption identity for metamaterials: experimental results and comparison with theory

Sohl, Christian; Larsson, Christer; Gustafsson, Mats; Kristensson, Gerhard

2007

CODEN:LUTEDX/(TEAT-7158)/1-10/(2007)
Revision No. 1: December 2007

A scattering and absorption identity for metamaterials — experimental results and comparison with theory

Christian Sohl, Christer Larsson, Mats Gustafsson, and Gerhard Kristensson

Electromagnetic Theory
Department of Electrical and Information Technology
Lund University
Sweden

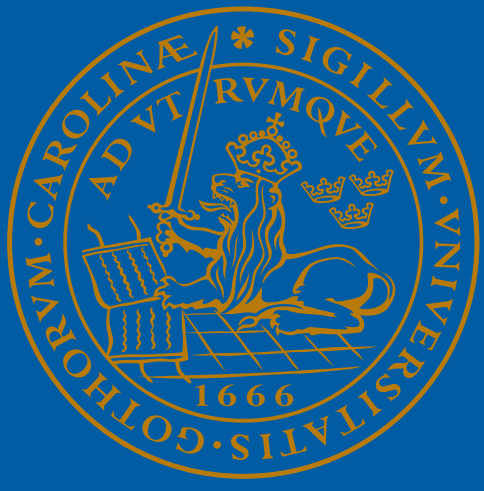

Christian Sohl, Mats Gustafsson, and Gerhard Kristensson
{Christian.Sohl,Mats.Gustafsson,Gerhard.Kristensson}@eit.lth.se

Department of Electrical and Information Technology
Electromagnetic Theory
P.O. Box 118
SE-221 00 Lund
Sweden

Christer Larsson
Christer.Larsson@saabgroup.com

Saab Communication AB
SE-581 88 Linköping
Sweden

Editor: Gerhard Kristensson

Abstract

A dispersion relation for the combined effect of scattering and absorption of electromagnetic waves is presented for a large class of linear and passive material models. By invoking the optical theorem, the result states that the extinction cross section integrated over all frequencies is equal to the static limit of the extinction volume. The present paper focuses on an attempt to experimentally verify this summation rule by measuring the monostatic radar cross section of a fabricated sample of metamaterial. In particular, the paper utilizes the idea that, for a specific class of targets, the scattered fields in the forward and backward directions coincide. It is concluded that the theoretical findings are in good agreement with the measurements performed in the frequency range $[3.2, 19.5]$ GHz.

1 Introduction

Since the contemporary discoveries of the Kramers-Kronig relations in 1926–27, dispersion relation techniques have been applied successfully to disparate wave phenomena to model the structural properties of wave interaction with matter [3, 8]. There are at least two main advantages of dispersion relations for the analysis of electromagnetic waves: i) they provide a consistency check of calculated quantities when the underlying mathematical model is known to satisfy causality, and ii) they may be used to verify whether a given mathematical model or an experimental outcome behaves causally or not. In addition, based on the field theoretical formalism in Ref. 11, dispersion relations can also be used to establish far-reaching connections between concepts of different physical meanings. A comprehensive review of dispersion relations in material modeling and scattering theory is presented in Ref. 17.

The optical theorem or forward scattering theorem relates the extinction cross section, or the combined effective area of absorption and scattering, to the forward scattering dyadic [10]. As a consequence, the magnitude and phase of the scattered field in a single direction solely determines the total power extinguished from an applied external field. In a series of papers in Refs. 15, 14 and 16, the use of a forward dispersion relation for the combined effect of scattering and absorption is exploited by invoking the optical theorem. In particular, it is established that the extinction cross section integrated over all frequencies is related to the static or long wavelength polarizability dyadics. This result is rather intriguing, and one of its many consequences on antennas show great potential for future applications [4, 5].

Although, the theory of broadband extinction of acoustic and electromagnetic waves by now is well established [14, 15], and numerical simulations show excellent agreement with the theory, its experimental verification is of scientific importance. Thus, the purpose of the present paper is to verify a certain aspect of these theoretical findings by measuring the monostatic radar cross section of a fabricated sample of metamaterial. The choice of considering a metamaterial is due to the fact that such materials by definition do not occur naturally, and if they can be manufactured, they are often claimed to possess extraordinary properties promising

for various engineering applications. In addition, experimental challenges associated with the extinction measurements are discussed in the paper. For example, to circumvent the weak signal strength of the scattered field in comparison with the incident field, the present paper utilizes the idea that, for a specific class of targets, the scattered field in the forward and backward directions coincide.

The main theoretical results used in this paper are summarized in Sec. 2, and the experimental results are developed and explained in Sec. 3. Finally, the paper is closed by some conclusions.

2 A scattering and absorption identity

Consider the direct scattering problem of a plane electromagnetic wave $\mathrm{e}^{\mathrm{i}k\hat{\boldsymbol{k}}\cdot\boldsymbol{x}}\hat{\boldsymbol{e}}$ (time dependence $\mathrm{e}^{-\mathrm{i}\omega t}$) of unit amplitude impinging in the $\hat{\boldsymbol{k}}$-direction on a target embedded in free space. The material of the scatterer is modeled by a set of linear and passive constitutive relations which are assumed to be independent of time. Let $\hat{\boldsymbol{k}}$ and $\hat{\boldsymbol{e}}$ be independent of the wave number $k \in [0, \infty)$, and introduce the differential cross section [7, 12]

$$\frac{\mathrm{d}\sigma}{\mathrm{d}\Omega}(k; \hat{\boldsymbol{k}} \curvearrowright \hat{\boldsymbol{x}}, \hat{\boldsymbol{e}}) = |\mathbf{S}(k; \hat{\boldsymbol{k}} \curvearrowright \hat{\boldsymbol{x}}) \cdot \hat{\boldsymbol{e}}|^2 \tag{2.1}$$

as a measure of the disturbance of the applied field due to the presence of the target. Here, the notation $\hat{\boldsymbol{k}} \curvearrowright \hat{\boldsymbol{x}}$ refers to the scattering of a plane wave into an outgoing spherical wave evaluated in the $\hat{\boldsymbol{x}}$-direction. The scattering dyadic $\mathbf{S}$ is independent of $\hat{\boldsymbol{e}}$, and it is defined in terms of the scattered electric field $\boldsymbol{E}_{\mathrm{s}}$ as [11]

$$\mathbf{S}(k; \hat{\boldsymbol{k}} \curvearrowright \hat{\boldsymbol{x}}) \cdot \hat{\boldsymbol{e}} = \lim_{x \to \infty} x \mathrm{e}^{-\mathrm{i}kx} \boldsymbol{E}_{\mathrm{s}}(k; \boldsymbol{x}),$$

where $x = |\boldsymbol{x}|$ denotes the magnitude of the position vector, and $\hat{\boldsymbol{x}} = \boldsymbol{x}/x$. In particular, 4π times the differential cross section in the backward direction, $\hat{\boldsymbol{x}} = -\hat{\boldsymbol{k}}$, yields the monostatic radar cross section [7, 12]

$$\sigma_{\mathrm{RCS}}(k; \hat{\boldsymbol{k}}, \hat{\boldsymbol{e}}) = 4\pi |\mathbf{S}(k; \hat{\boldsymbol{k}} \curvearrowright -\hat{\boldsymbol{k}}) \cdot \hat{\boldsymbol{e}}|^2.$$

A target's overall scattering properties are commonly quantified by the scattering cross section σ_{s}, defined as the total power scattered in all directions divided by the incident power flux. It is obtained by integrating (2.1) over the unit sphere with respect to the $\hat{\boldsymbol{x}}$-direction, *i.e.*,

$$\sigma_{\mathrm{s}}(k; \hat{\boldsymbol{k}}, \hat{\boldsymbol{e}}) = \int \frac{\mathrm{d}\sigma}{\mathrm{d}\Omega}(k; \hat{\boldsymbol{k}} \curvearrowright \hat{\boldsymbol{x}}, \hat{\boldsymbol{e}}) \, \mathrm{d}\Omega. \tag{2.2}$$

Based on (2.2), the extinction cross section $\sigma_{\mathrm{ext}} = \sigma_{\mathrm{s}} + \sigma_{\mathrm{a}}$ is defined as the sum of the scattering and absorption cross sections, where the latter is a measure of the absorbed power in the target [1]. The extinction cross section is also determined from the knowledge of the scattering dyadic in the forward direction, $\hat{\boldsymbol{x}} = \hat{\boldsymbol{k}}$, *viz.*,

$$\sigma_{\mathrm{ext}}(k; \hat{\boldsymbol{k}}, \hat{\boldsymbol{e}}) = \frac{4\pi}{k} \operatorname{Im}\left\{ \hat{\boldsymbol{e}}^* \cdot \mathbf{S}(k; \hat{\boldsymbol{k}} \curvearrowright \hat{\boldsymbol{k}}) \cdot \hat{\boldsymbol{e}} \right\}, \tag{2.3}$$

where an asterisk denotes the complex conjugate. Relation (2.3) is known as the optical theorem, and it is applicable to many different wave phenomena such as acoustic waves, electromagnetic waves, and elementary particles [10, 17].

From the integral representations in Ref. 18, or the discussion on p. 11 in Ref. 12, it follows that, for a planar and infinitely thin target subject to an arbitrary field incident at normal incidence, the forward and backward scattering dyadics are equal, *i.e.*,

$$\mathbf{S}(k;\hat{\boldsymbol{k}} \curvearrowright \hat{\boldsymbol{k}}) \cdot \hat{\boldsymbol{e}} = \mathbf{S}(k;\hat{\boldsymbol{k}} \curvearrowright -\hat{\boldsymbol{k}}) \cdot \hat{\boldsymbol{e}}. \tag{2.4}$$

For this specific class of targets, (2.4) enables extinction measurements to be carried out by simply detecting the scattered field in the backward direction. Of course, both the magnitude and phase of the scattered field have to be identified. In particular, (2.4) implies that the differential cross section in the forward and backward directions are identical, *i.e.*,

$$\frac{\mathrm{d}\sigma}{\mathrm{d}\Omega}(k;\hat{\boldsymbol{k}} \curvearrowright \hat{\boldsymbol{x}}, \hat{\boldsymbol{e}}) = \frac{\mathrm{d}\sigma}{\mathrm{d}\Omega}(k;\hat{\boldsymbol{k}} \curvearrowright -\hat{\boldsymbol{x}}, \hat{\boldsymbol{e}}).$$

Note that more general methods must be introduced to experimentally determine the forward scattered field when any of the above-stated assumptions are violated, see pp. 320–323 in Ref. 1.

A dispersion relation for the combined effect of scattering and absorption of electromagnetic waves is derived in Ref. 15 from the holomorphic properties of the forward scattering dyadic [6]. The result is a summation rule for the extinction cross section valid for a large class of linear and passive targets, *viz.*,

$$\int_0^\infty \frac{\sigma_{\mathrm{ext}}(k;\hat{\boldsymbol{k}},\hat{\boldsymbol{e}})}{k^2}\,\mathrm{d}k = 2\pi^2 \varrho(0;\hat{\boldsymbol{k}},\hat{\boldsymbol{e}}), \tag{2.5}$$

where the static limit on the right hand side of (2.5) is non-negative. Here, the extinction volume $\varrho(k;\hat{\boldsymbol{k}},\hat{\boldsymbol{e}})$ is defined by the complex-valued quantity

$$\varrho(k;\hat{\boldsymbol{k}},\hat{\boldsymbol{e}}) = \frac{\hat{\boldsymbol{e}}^* \cdot \mathbf{S}(k;\hat{\boldsymbol{k}} \curvearrowright \hat{\boldsymbol{k}}) \cdot \hat{\boldsymbol{e}}}{k^2}. \tag{2.6}$$

In particular, the extinction cross section is related to the imaginary part of the extinction volume via the optical theorem (2.3), $\sigma_{\mathrm{ext}}(k,\hat{\boldsymbol{k}},\hat{\boldsymbol{e}}) = 4\pi k \operatorname{Im} \varrho(k;\hat{\boldsymbol{k}},\hat{\boldsymbol{e}})$. The extinction volume satisfies the Hilbert transform or the improper integral [19]

$$\varrho(k;\hat{\boldsymbol{k}},\hat{\boldsymbol{e}}) = \frac{1}{\mathrm{i}\pi}\mathcal{P}\int_{-\infty}^{\infty} \frac{\varrho(k';\hat{\boldsymbol{k}},\hat{\boldsymbol{e}})}{k'-k}\,\mathrm{d}k', \tag{2.7}$$

where $\mathcal{P}$ denotes the Cauchy principal value. The fact that the extinction cross section is non-negative implies that the left hand side of (2.5) can be estimated from below by the corresponding integral over $[k_1, k_2]$, *viz.*,

$$\int_{k_1}^{k_2} \frac{\sigma(k;\hat{\boldsymbol{k}},\hat{\boldsymbol{e}})}{k^2}\,\mathrm{d}k \le \int_0^\infty \frac{\sigma_{\mathrm{ext}}(k;\hat{\boldsymbol{e}},\hat{\boldsymbol{k}})}{k^2}\,\mathrm{d}k = 2\pi^2 \varrho(0;\hat{\boldsymbol{k}},\hat{\boldsymbol{e}}), \tag{2.8}$$

where σ denotes any of σ_{ext}, σ_{s} and σ_{a}. The interpretation of (2.8) is that there is only a limited amount of scattering and absorption available in $[k_1, k_2]$, and that this amount is bounded from above by the static limit of the extinction volume [15, 16].

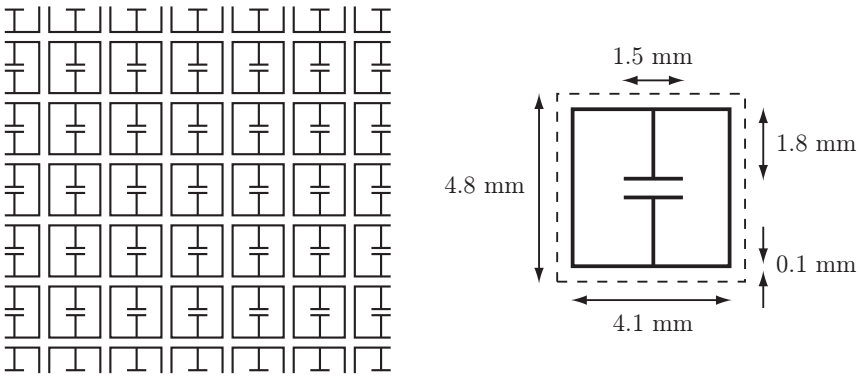

Figure 1: A section of the fabricated sample (left figure) and a close-up of the square unit cell (right figure). The line width of the printed circuit board is 0.1 mm.

3 Experimental results

In this section, measurements of the extinction cross section are presented for a fabricated sample of metamaterial. The sample design and experimental setup are described, and the outcome of the measurements is compared with the theoretical results in Sec. 2. Throughout this section, the quantities introduced in Sec. 2 are denoted by the same dependent variables also when they are formulated in the frequency $f = \mathrm{c}_0 k/2\pi$ (c_0 is the speed of light in vacuum).

3.1 Sample design and experimental setup

The fabricated sample is designed as a single-layer planar array of capacitive resonators tuned to be resonant at 8.5 GHz. It consists of 29×29 unit cells supported by a square FR4 substrate of edge length $a = 140$ mm and thickness 0.3 mm, see Fig. 1. The relative dielectric constant of the substrate varies between 4.2 and 4.4 in the frequency range $f \in [3.2, 19.5]$ GHz, with an overall loss tangent less than $4.8 \cdot 10^{-3}$. The sample design in Fig. 1 is commonly referred to in the literature as a negative permittivity metamaterial [13].

Monostatic radar cross section measurements are performed in the anechoic chamber at Saab Bofors Dynamics, Linköping, Sweden. The sample is mounted on an expanded polystyrene sample holder and placed on a pylon. Dual polarized ridged circular waveguide horns are positioned at a distance of 3.55 m from the sample, see Fig. 2, and an Agilent Performance Network Analyzer (PNA) is used for transmitting a continuous wave without online hard or software gating. The polarizations of the transmitted and received fields are parallel to the capacitors in the printed circuit, *i.e.*, vertically positioned in Fig. 1. The original frequency range $[2, 20]$ GHz is reduced to $[3.2, 19.5]$ GHz due to the range domain filtering of the data. The latter frequency interval is sampled with 7246 equidistant points corresponding to an unambiguous spatial range of 66.7 m which is sufficient to avoid influence of any room reverberations.

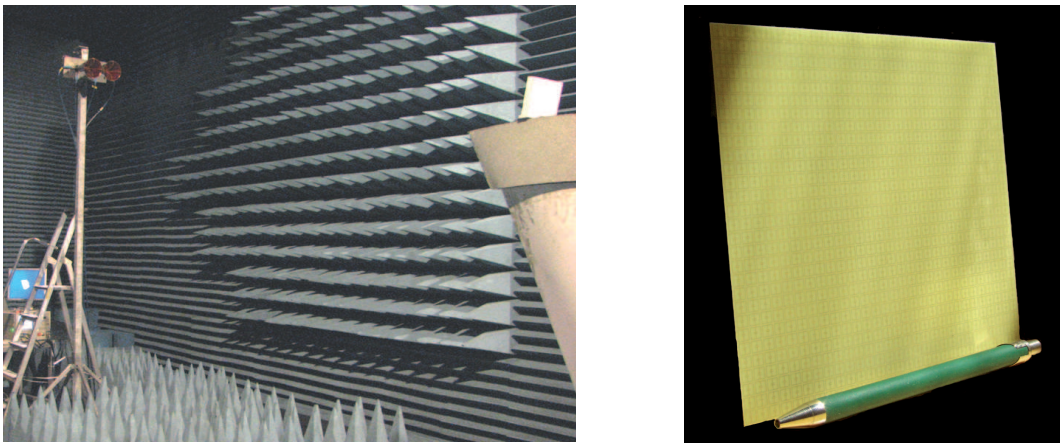

Figure 2: The experimental setup in the anechoic chamber (left figure) and the fabricated sample with 29×29 unit cells supported by a square FR4 substrate of edge length 140 mm (right figure).

Calibration including both amplitude and phase is performed using a metal plate with the same outer dimensions as the sample in Fig. 2. A physical optics approximation for a perfectly electric conducting plate is adopted as the calibration reference, see p. 523 in Ref. 12. In order to validate the calibration, a method of moments calculation is also performed. It is concluded that the method of moments solution does not deviate significantly from the physical optics approximation. In addition to being a calibration reference, the metal plate is also used to align the experimental setup using the specular reflection of the plate.

The data from the measurements are processed by a coherent subtraction of the background followed by a calibration using the physical optics approximation. The frequency domain data is then transformed to the range domain, where the response from the sample is selected from the range profile using a 1.1 m spatial gate. Finally, the selected data is transformed back to the frequency domain.

3.2 Measurement results and comparison with theory

The monostatic radar cross section of the sample is depicted by the solid line on the left hand side in Fig. 3. In the figure, the first resonance at $f_0 \approx 8.5\,\text{GHz}$ is observed as well as an increase in the monostatic radar cross section with frequency, consistent with the specular reflection of the sample. As the sample is sufficiently thin, the forward scattering dyadic is approximated by the scattering dyadic in the backward direction. In particular, this approximation is used to calculate the extinction cross section via the optical theorem (2.3). The result is depicted on the right hand side in Fig. 3. From the figure it is seen that the extinction cross section is non-negative confirming the validity of (2.4) since phase deviations in the scattering dyadic introduce significant errors in the extinction cross section.

The forward scattering dyadic is also used to determine the extinction volume,

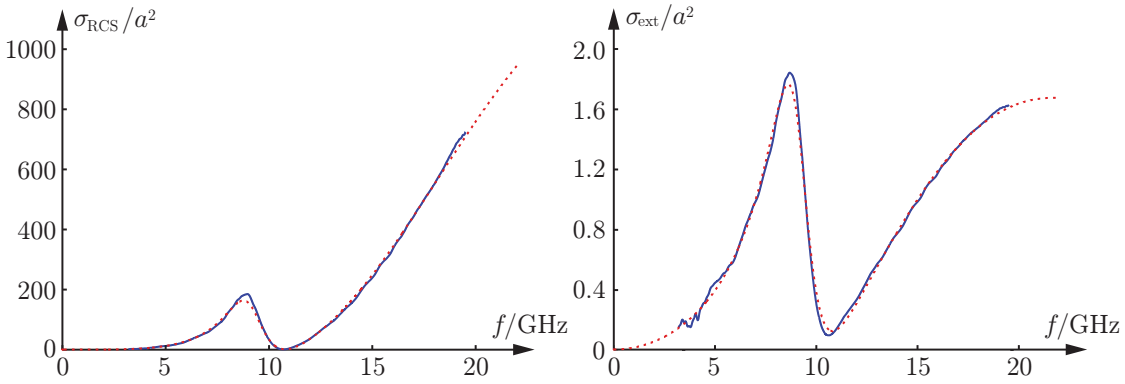

Figure 3: The monostatic radar cross section (left figure) and the extinction cross section (right figure) in units of the forward projected area a^2. The solid lines correspond to measured data whereas the dashed lines are given by (3.2).

and the result is depicted on the left hand side in Fig. 4. From the figure it is observed that the real-valued part of the extinction volume vanishes at the resonance frequency $f_0 \approx 8.5\,\mathrm{GHz}$, whereas at the same frequency, the corresponding imaginary part attains its maximum value. This observation can be understood by approximating the resonance on the left hand side in Fig. 4 with the Lorentz resonance model, see pp. 228–232 in Ref. 1, *i.e.*,

$$\varrho(f;\hat{\boldsymbol{k}},\hat{\boldsymbol{e}}) \propto \frac{f_0^2 + \mathrm{i}f\nu_0}{f_0^2 + 2\mathrm{i}ff_0/Q_0 - f^2}, \tag{3.1}$$

where Q_0 denotes the Q-factor of the resonance. Also, note in Fig. 4 that the frequency scaling in (2.6) amplifies the noise in the measurements for low frequencies.

The function $\zeta(k;\hat{\boldsymbol{k}},\hat{\boldsymbol{e}}) = 4\pi\,\mathrm{Im}\,\varrho(k;\hat{\boldsymbol{k}},\hat{\boldsymbol{e}})/k$, corresponding to the integrand in (2.5), is depicted on the right hand side in Fig. 4. Compared with the figure on the left hand side, additional noise amplification for low frequencies is observed. The shaded area on the right hand side is estimated by numerical integration to $7.1\,\mathrm{cm}^3$ and indicated by the dot in the left figure. Since ζ is non-negative, the value $7.1\,\mathrm{cm}^3$ provides, according to (2.8), a lower bound on the static limit of the extinction volume. Obviously, this static limit is underestimated by the integral since it is unlikely that ζ vanishes identically outside the frequency range $[3.2, 19.5]\,\mathrm{GHz}$.

The extinction volume is also used to verify that the experimental outcome behaves causally in the sense that the extinction volume satisfies (2.7). In Fig. 5, it is observed that the Hilbert transform resembles the overall frequency dependence of the real and imaginary parts of the extinction volume. However, it is clear from the figure that the finite frequency interval of the measured data limits its usefulness as a method of reconstructing an unknown component of a holomorphic function.

A feasible technique to approximate the extinction volume is to use meromorphic functions with roots and zeroes in the lower half of the complex f-plane. Numerical tests using the algorithm in Ref. 9 indicate that it is sufficient to consider rational functions with numerator and denominator of second and fourth degree, respectively.

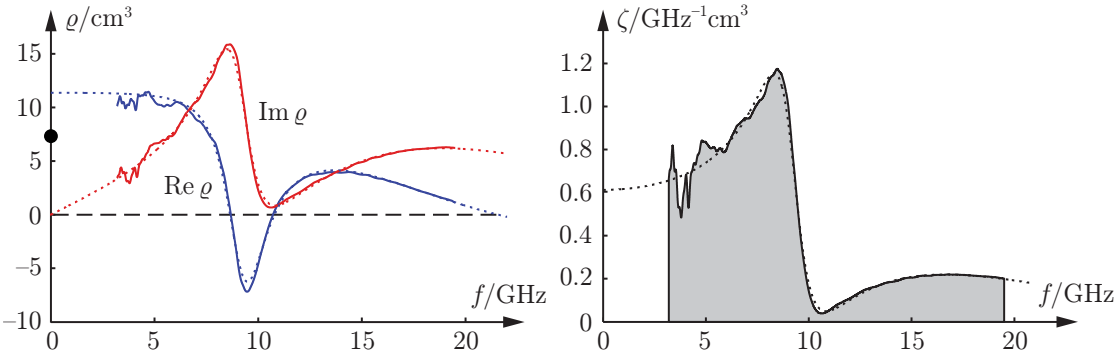

Figure 4: The extinction volume (left figure) and $\zeta(k;\hat{\boldsymbol{k}},\hat{\boldsymbol{e}}) = 4\pi \operatorname{Im} \varrho(k;\hat{\boldsymbol{k}},\hat{\boldsymbol{e}})/k$ (right figure). The solid lines correspond to measured data whereas the dashed lines are given by (3.2). The shaded area on the right hand side is marked with a dot in the left figure.

Such functions can be represented by the sum of two Lorentz resonance models via

$$\varrho_{\text{appr}}(f;\hat{\boldsymbol{k}},\hat{\boldsymbol{e}}) = \sum_{n=1}^{2} \varrho_n \frac{f_n^2 + \mathrm{i} f \nu_n}{f_n^2 + 2\mathrm{i} f f_n/Q_n - f^2}. \tag{3.2}$$

The approximation (3.2) is depicted by the dotted lines in Fig. 4. Here, $f_1 = 9.3\,\text{GHz}$, $Q_1 = 7.8$, $\varrho_1 = 1.3\,\text{cm}^3$, and $\nu_1 = -27\,\text{GHz}$ for the first term, and $f_2 = 20\,\text{GHz}$, $Q_2 = 1.6$, $\varrho_2 = 10\,\text{cm}^3$, and $\nu_2 = 3.6\,\text{GHz}$ for the second term. In particular, the static limit of (3.2) is given by $\varrho_1 + \varrho_2 \approx 11\,\text{cm}^3$. The associated meromorphic approximations of the monostatic radar cross section and the extinction cross section follow from (3.2) and the definitions in Sec. 2. These approximations are represented by the dotted lines in Figs. 3 and 4, and it is concluded that the approximations are in good agreement with the experimental results.

The approximation in (3.2) is also used to establish a sharper bound on the static limit of the extinction volume. In fact, the shaded area $7.1\,\text{cm}^3$ on the right hand side of Fig. 4 should be compared with the corresponding area $9.8\,\text{cm}^3$ obtained by integrating the dotted line over the frequency range $[0, 22]\,\text{GHz}$. The lower bound $9.8\,\text{cm}^3$ is quite close to the static limit $11\,\text{cm}^3$, which would be the true value of $\varrho(0;\hat{\boldsymbol{k}},\hat{\boldsymbol{e}})$ if the extinction volume on the left hand side of Fig. 4 is completely determined by the dotted line. The fact that the dotted line on the right hand side of Fig. 4 is non-zero in the static limit is also supported by the analysis of the lossy transmission problem on pp. 191–192 in Ref. 2.

4 Conclusions

This present paper reports on measurements of the extinction cross section and the extinction volume for a fabricated sample of a negative permittivity metamaterial. It is experimentally verified that the extinction cross section integrated over

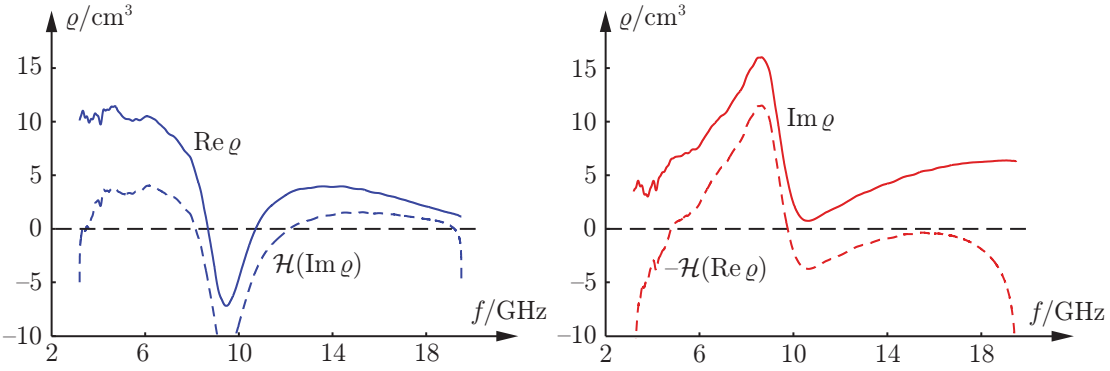

Figure 5: The real and imaginary parts of the extinction volume (solid lines) and the corresponding reconstructed quantities using the Hilbert transform $\mathcal{H}$ (dashed lines).

the frequency interval $[3.2, 19.5]$ GHz yields a lower bound on the static limit of the extinction volume. Also, by using the Hilbert transform and the meromorphic approximation in (3.2), it is made plausible that the extinction volume indeed is a holomorphic function in the upper half part of the complex k-plane and there satisfies the asymptotic behavior discussed in Ref. 15. Among other things, the experimental results in this paper are important for the support of the far-reaching conclusion made in Ref. 16: there is no fundamental difference between metamaterials and naturally formed substances with respect to the absorption and scattering over a frequency interval.

Similar measurements on split ring resonators will be presented in a forthcoming paper. Forward scattering measurements on extended targets introduce further experimental challenges that also will be addressed in the future.

Acknowledgments

The financial support by the Swedish Research Council is gratefully acknowledged. The authors also thank Carl-Gustaf Svensson and Mats Andersson at Saab Bofors Dynamics, Linköping, Sweden, for generous hospitality and practical assistance throughout the measurements.

References

[1] C. F. Bohren and D. R. Huffman. *Absorption and Scattering of Light by Small Particles*. John Wiley & Sons, New York, 1983.

[2] G. Dassios and R. Kleinman. *Low frequency scattering*. Oxford University Press, Oxford, 2000.

[3] R. de L. Kronig. On the theory of dispersion of X-rays. *J. Opt. Soc. Am.*, **12**(6), 547–557, 1926.

[4] M. Gustafsson, C. Sohl, and G. Kristensson. Physical limitations on antennas of arbitrary shape. *Proc. R. Soc. A*, **463**, 2589–2607, 2007.

[5] M. Gustafsson, C. Sohl, and G. Kristensson. Physical limitations on antennas of arbitrary shape. Technical Report LUTEDX/(TEAT-7153)/1–37/(2007), Lund University, Department of Electrical and Information Technology, P.O. Box 118, S-221 00 Lund, Sweden, 2007. http://www.eit.lth.se.

[6] E. Hille. *Analytic Function Theory*, volume 1. Chelsea Publishing Company, New York, second edition, 1982.

[7] E. F. Knott, J. F. Shaeffer, and M. T. Tuley. *Radar Cross Section*. SciTech Publishing Inc., 5601 N. Hawthorne Way, Raleigh, NC 27613, 2004.

[8] M. H. A. Kramers. La diffusion de la lumière par les atomes. *Atti. Congr. Int. Fis. Como*, **2**, 545–557, 1927.

[9] E. C. Levi. Complex-curve fitting. *IRE Trans. on Automatic Control*, **4**, 37–44, 1969.

[10] R. Newton. Optical theorem and beyond. *Am. J. Phys*, **44**, 639–642, 1976.

[11] R. G. Newton. *Scattering Theory of Waves and Particles*. Dover Publications, New York, second edition, 2002.

[12] G. T. Ruck, D. E. Barrick, W. D. Stuart, and C. K. Krichbaum. *Radar Cross-Section Handbook*, volume 1. Plenum Press, New York, 1970.

[13] D. Schurig, J. J. Mock, and D. R. Smith. Electric-field-coupled resonators for negative permittivity metamaterials. *Appl. Phys. Lett.*, **88**, 041109, 2006.

[14] C. Sohl, M. Gustafsson, and G. Kristensson. The integrated extinction for broadband scattering of acoustic waves. Accepted for publication in J. Acoust. Soc. Am., 2007.

[15] C. Sohl, M. Gustafsson, and G. Kristensson. Physical limitations on broadband scattering by heterogeneous obstacles. *J. Phys. A: Math. Theor.*, **40**, 11165–11182, 2007.

[16] C. Sohl, M. Gustafsson, and G. Kristensson. Physical limitations on metamaterials: Restrictions on scattering and absorption over a frequency interval. *J. Phys. D: Applied Phys.*, **40**, 7146–7151, 2007.

[17] C. Sohl. *Dispersion Relations for Extinction of Acoustic and Electromagnetic Waves*. Licentiate thesis, Lund University, Department of Electrical and Information Technology, P.O. Box 118, S-221 00 Lund, Sweden, 2007. http://www.eit.lth.se.

[18] S. Ström. Introduction to integral representations and integral equations for time-harmonic acoustic, electromagnetic and elastodynamic wave fields. In V. V. Varadan, A. Lakhtakia, and V. K. Varadan, editors, *Field Representations and Introduction to Scattering*, volume 1 of *Handbook on Acoustic, Electromagnetic and Elastic Wave Scattering*, chapter 2, pages 37–141. Elsevier Science Publishers, Amsterdam, 1991.

[19] E. C. Titchmarsh. *Introduction to the Theory of Fourier Integrals*. Oxford University Press, Oxford, second edition, 1948.